Available online at www.sciencedirect.com
SCIENCE DIRECT®

Journal of the European Ceramic Society 23 (2003) 1585–1591
www.elsevier.com/locate/jeurceramsoc

Defect profile and microstructural development in SnO_2-based varistors

J. Fayat, M.S. Castro*

Institute of Materials Science and Technology (INTEMA), (CONICET—Universidad Nacional de Mar del Plata), Av. Juan B. Justo 4302, (B7608FDQ) Mar del Plata, Argentina

Received 1 May 2002; received in revised form 30 September 2002; accepted 20 October 2002

Abstract

The microstructural development and the stabilised valence of the ions added to SnO_2 were analysed. Aiming at a better interpretation of the involved phenomena, the effects on grain growth, secondary phase formation and structure of adding Co_3O_4, ZnO, MnO_2, Sb_2O_3, or Nb_2O_5 have been studied. We found that cobalt, zinc and manganese stabilise as Co^{+2}, Zn^{+2} and Mn^{+2} in the lattice, favouring the oxygen vacancy apparition and then, the grain growth and the potential barrier formation. Sb_2O_3 or Nb_2O_5 reduces the total oxygen vacancy concentration and the grain growth. Sb_2O_3 addition favours the $CoSnO_3$ particle formation and Nb_2O_5 favours the formation of particles with an intermediate composition between $CoSnO_3$ and Co_2SnO_4 in systems with Co_3O_4. These particles could also control the sintering and grain growth rates.

Keywords: Defects; Grain growth; Microstructure-final; SnO_2; Varistors

1. Introduction

Varistors are semiconductor devices whose current–voltage characteristics are highly non-linear. Their primary function is to sense and limit transient voltage surges and to do so repeatedly without being destroyed.[1,2] The non-linear current–voltage (I–V) characteristic is expressed by the equation $I = V^{\alpha}$, where α is the non-linearity coefficient.[3] Ohmic resistors have $\alpha = 1$ while ideal varistors have infinite values of α.

Commercial varistors are based on SiC or in ZnO. SiC based varistors have very low non-linearity coefficient ($\alpha = 5$) while ZnO-based varistors have very high non-linearity coefficient ($\alpha = 50$).[4] At the same time, other varistor systems have been studied, because of the need for even better properties. Among them, systems based on $SrTiO_3$,[5] TiO_2,[6,7] and SnO_2[8–10] have been described in the literature.

Tin oxide is a semiconductor with crystalline structure of rutile type and has very low densification rate due to its high surface diffusion at low temperatures and high SnO_2 partial pressure at high temperatures.[11] Due to this particular property, SnO_2 has been extensively used as gas sensors.[12,13] Pianaro et al.[8] reported that doping by Co_2O_3 and Nb_2O_5 drastically improve the sinterability of SnO_2, and they observed highly non-linear current–voltage characteristic. At present it is known that several dopants (such as CoO, MnO_2) form solid solutions with SnO_2 and create charged oxygen vacancies at sintering temperatures. These oxygen vacancies as well as Mn^{+2}, Mn^{+3} or Co^{+2} ions substituting Sn^{+4} are segregated at the grain boundaries and improve mass transport leading to densification and grain growth.[14] Other additives (such as Bi_2O_3 and CuO) improve SnO_2 densification by forming a reactive liquid phase.[10,15] On the other hand, it was reported that Sb_2O_3 or Nb_2O_5 decreases the SnO_2 sinterability.[16,17]

The goal of the present work is to investigate the influence of Co_3O_4, ZnO, MnO_2, Sb_2O_3, Nb_2O_5 on the microstructure development, on the secondary phases formation, on the lattice volume, on the defect structure, and on the electrical behaviour. Also, the stabilised valence of the ions added in the SnO_2 lattice is analysed.

2. Experimental procedure

Analytical grades of SnO_2 (Aldrich, average particle size 0.42 μm, specific area 5.5 m^2/g), Co_3O_4 (Merck),

* Corresponding author.
E-mail address: mcastro@fi.mdp.edu.ar (M.S. Castro).

0955-2219/02/$ - see front matter
PII: S0955-2219(02)00405-3

ZnO (Mallinckrodt), MnO_2 (Merck), Sb_2O_3 (Carlo Erba), Nb_2O_5 (Fluka AG), were used as precursors for processing SnO_2 based varistors. Selected compositions are listed in Table 1. Starting powders were mixed in alcoholic medium by stirring in a high-speed turbine at 6000 rpm for 5 min. Then, slurries were dried at 65 °C until constant weight. After being cooled down, mixtures were crushed into powder and sieved through a 43 μm mesh screen. Finally, samples were pressed (200 MPa) into disks of 1 cm in diameter and 0.15 cm thick. They were sintered at 1300 °C for 2 h (heating and cooling rate: 3 °C/min).

In order to calculate the apparent density of the sintered samples, Archimedes method was applied. Microstructural characteristics of the polished and thermally etched samples were observed by scanning electron microscopy (SEM) using a Philips 505 microscope, while elemental analyses (EDS) were carried out with an EDAX (Topcon SM-300 and PGT digital spectrometer). By using the Soft Imaging System AnalySIS® 3.0 software, evaluation of the average grain size was performed on SEM images. X-ray diffraction (XRD) analysis of the SnO_2 was carried out on sintered samples, using a Philips PW 1050/25 equipment with CuK_α radiation and a Ni filter, at 40 kV and 30 mA. From XRD reflections corresponding to the (110) and (101) planes, a qualitative analysis of the cell distortion in SnO_2 samples was made. These signals were located in a value of the 2θ angle (radiation CuK_α)≈26.61° [(110) plane] and $2\theta \approx 33.89°$ [(101) plane]. The spacings (d_1 and d_2) of the crystallographic planes [(110) and (101)] were determined using the Bragg condition. To quantify the cell distortion, c and a parameters for the tetragonal system were calculated with the following equations:[18]

$$1/d_1 = 2/a^2 \tag{1}$$

$$1/d_2 = 1/a^2 + 1/c^2 \tag{2}$$

To achieve a precise data collection, scanning was performed at 0.125°/min and 2θ angle ranging from 26 to 28° and from 33 to 35°.

A Bruker ER-200 (Band X) EPR spectroscope with a variable gain between 2×10^4 and 8×10^3, a power of 5 dB and modulation amplitude of 6.3 Gpp was used to characterise the paramagnetic species present in the sintered and grounded samples at room temperature. The EPR signal intensities were labelled as double integrated intensities (DII) calculated from the empirical relation applied by Murugaraj et al.:[19]

$$\begin{aligned} \mathrm{DII} = &\left[(\textit{signal height})\right]\cdot(\textit{signal width}) \\ &/\left[(\textit{sample mass})\cdot(\textit{gain})\right. \\ &\left.\cdot(\textit{modulation amplitude})\cdot(\textit{power})^{1/2}\right] \end{aligned} \tag{3}$$

Samples were silver painted for the electrical characterisation. Current–voltage characteristics at room temperature were obtained using a stabilised electrical source (0–220 V) and a Keithley 614 electrometer for small currents, while for large currents a multimeter was used. The electrical breakdown field was obtained at 1 mA cm^{-2} current density.The grain voltage (V_g) was estimated as:

$$V_g = E_r/n \tag{4}$$

where, E_r is the breakdown voltage, and n is the number of grains in series of a given sample of width L and mean grain size G,

$$n = L/G \tag{5}$$

The effective barrier voltage (V_e) for the sintered samples was

$$V_e = V_g/\mathrm{BG}\cdot 100, \tag{6}$$

where, BG is the SnO_2 band gap (about 3.5eV).[20]

3. Results and discussion

Table 2 shows the densities of the sintered samples obtained through the Archimedes method. The sample composed by SnO_2 without additives presented a low densification after the sintering process. However, addition of Co_3O_4, MnO_2 or ZnO increased the material density. On the other hand, the Nb_2O_5 or Sb_2O_3 addition produced a detrimental effect on the sample density. These changes in the sample densities could be explained through modifications in the oxygen vacancy concentration, as it will be explained below.

Table 1
Sample composition (%mol)

Sample	SnO_2	Co_3O_4	ZnO	MnO_2	Sb_2O_3	Nb_2O_5
Sn	100	–	–	–	–	–
SnCo	99.66	0.34	–	–	–	–
SnZn	99.04	–	0.96	–	–	–
SnMn	99.06	–	–	0.94	–	–
SnCoSb	99.56	0.34	–	–	0.1	–
SnCoNb	99.56	0.34	–	–	–	0.1

Table 2
Densities of the sintered samples

Sample	Density (g cm^{-3})	Relative density (%)
Sn	4.42	63.7
SnCo	6.76	97.3
SnZn	6.60	95.0
SnMn	6.74	96.9
SnCoSb	6.65	95.7
SnCoNb	6.56	94.3

From the XRD analysis only peaks corresponding to SnO_2 were detected, no other crystalline phase besides cassiterite (SnO_2) was observed indicating that the systems were single phase within the detection precision of X-ray diffraction. XRD analysis was also used to detect the SnO_2 lattice distortion by the foreign ions presence. Table 3 shows the lattice parameters obtained from the Bragg equations. From the table a deformation in the lattice volume by the oxides addition was observed. These changes are influenced by the ion valence stabilised in the tin oxide lattice. An increase in the lattice volume with the Co_3O_4, ZnO or MnO_2 addition was detected. On the other hand, a diminution in the lattice volume with the Sb_2O_3 or Nb_5O_5 was observed from the experimental results.

In order to explain these changes, possible replace equations in the tin oxide are discussed as follows. In the Co_3O_4 addition the possible substitution equations are:

$$Co_3O_4 \rightarrow CoO + Co_2O_3 \quad (7)$$

then,

$$CoO \rightarrow Co''_{Sn} + V_O^{\cdot\cdot} + O_O \quad (8)$$

$$Co_2O_3 \rightarrow 2Co'_{Sn} + V_O^{\cdot\cdot} + 3O_O^x \quad (9)$$

$$V_O^{\cdot\cdot} + e' \rightarrow V_O^{\cdot} \quad (10)$$

$$V_O^x \rightarrow V_O^{\cdot} + e' \quad (11)$$

From these equations, cobalt could stabilise as Co^{+2} (ionic radius 0.72Å)[21] or as Co^{+3} (ionic radius 0.63Å).[21] From Table 3 cobalt addition produced an increase in the lattice volume respect to the SnO_2 sample. This means that cobalt must stabilise as Co^{+2} in the SnO_2 lattice, because this ion has a major ionic radius (remember that Sn^{+4} radius is 0.71 Å),[21] also Co^{+3} could exist at the grain boundary and at minor concentration at grain . This result is in accordance with previous investigations employing UV–Vis DRS.[10] Then, from Eq. (8) an increase in the oxygen vacancy concentration with the cobalt addition was produced favouring the varistor densification.

Table 3
SnO_2 lattice parameters of the sintered samples

Sample	a (Å)	c (Å)	$V = a^2.c$ (Å^3)
Sn	4.738	3.185	71.499
SnCo	4.738	3.188	71.566
SnZn	4.741	3.185	71.589
SnMn	4.744	3.185	71.680
SnCoSb	4.732	3.184	71.296
SnCoNb	4.732	3.182	71.251

In the ZnO addition, the substitution equations are:

$$ZnO \rightarrow Zn''_{Sn} + V_O^{\cdot\cdot} + O_O^x \quad (12)$$

$$V_O^{\cdot\cdot} + e' \rightarrow V_O^{\cdot} \quad (13)$$

$$V_O^x \rightarrow V_O^{\cdot} + e' \quad (14)$$

In this case, zinc ions could stabilise only as Zn^{+2} (ionic radius 0.74Å) [21] and, as a consequence, the lattice volume increased (Sn^{+4} radius 0.71 Å). [21]

In the MnO_2 addition several ions could stabilise. It is known that during the sintering process the following reactions could occur:[10]

$$2\ MnO_2 \rightarrow Mn_2O_3 + 1/2O_2 \quad (15)$$

$$Mn_2O_3 \rightarrow 2\ MnO + 1/2\ O_2 \quad (16)$$

Then, the possible substitution equations are

$$MnO \rightarrow Mn''_{Sn} + V_O^{\cdot\cdot} + O_O^x \quad (17)$$

$$MnO_2 \rightarrow Mn_{Sn}^x + 2O_O^x \quad (18)$$

$$Mn_2O_3 \rightarrow 2Mn'_{Sn} + V_O^{\cdot\cdot} + 3O_O^x \quad (19)$$

$$V_O^{\cdot\cdot} + e' \rightarrow V_O^{\cdot} \quad (20)$$

$$V_O^x \rightarrow V_O^{\cdot} + e' \quad (21)$$

Mn^{+4} and Mn^{+3} have smaller ionic radii than Sn^{+4} (0.60, 0.66, and 0.71 Å, respectively),[21] but Mn^{+2} radius is higher (0.80 Å).[21] From Table 3 an increases in the SnO_2 volume lattice with the manganese addition was observed, indicating that manganese was stabilised as Mn^{+2} in the SnO_2 lattice. This result is according to previous studies by UV–Vis DRS.[10]

As can be seen from the above equations the addition of Co_3O_4, ZnO, MnO_2, which stabilise as Co^{+2}, Zn^{+2}, and Mn^{+2} in the lattice, produced an increase in the oxygen vacancy concentration, improving the mass transport and favouring the SnO_2-based varistor densification.

In the Sb_2O_3 addition the possible substitution equations are:

$$Sb_2O_3 \rightarrow 2\ Sb'_{Sn} + V_O^{\cdot\cdot} + 3O_O^x \quad (22)$$

$$Sb_2O_5 \rightarrow 2\ Sb_{Sn}^{\cdot} + 2\ e' + 4O_O^x + 1/2\ O_2(g) \quad (23)$$

From Table 3, Sb_2O_3 addition to SnCo system produced a diminution in the lattice volume. This diminution in the volume could not be produced by the Sb^{+3} stabilisation (Sb^{+3} radius is 0.76 Å[21] and Sn^{+4} radius is 0.71 Å).[21] According to the volume lattice data and the ionic radii, Sb^{+5} stabilisation was produced (Sb^{+5} radius is 0.62Å).[21] To explain this behaviour it is necessary to point out that Sb_2O_5 is the stable form up to 970 °C, but Sb_2O_3 is more stable at higher temperatures.

However, the Sb^{+5}/Sb^{+3} ratio will depend both on the temperature and on the concentration at ambient oxygen.[22] Then, it is possible that during the cooling process the transformation of Sb^{+3} into Sb^{+5} takes place.

In the Nb_2O_5 addition the following equations could occur:

$$2\ Nb_2O_5 \rightarrow 4\ Nb_{Sn}^{\cdot} + V_{Sn}^{''''} + 10\ O_O^x \quad (24)$$

$$V_{Sn}^{''''} + 2\ V_O^{\cdot\cdot} \rightarrow 2\ V_O^{\cdot} + V_{Sn}^{''} \quad (25)$$

or

$$Nb_2O_5 \rightarrow 2\ Nb_{Sn}^{\cdot} + 2\ e' + 4O_O^x + 1/2O_2(g) \quad (26)$$

$$V_O^{\cdot\cdot} + e' \rightarrow V_O^{\cdot} \quad (27)$$

Experimental data were insufficient to select one of the two possible substitution equations in the Nb_2O_5 addition. In both cases, Nb^{+5} has a lower ionic radius (0.69 Å)[21] than Sn^{+4} (0.71 Å),[21] and produces a diminution in the tin oxide lattice (see Table 3). From these annihilation equations of oxygen vacancies with oxygen was produced. Then, a diminution in the density samples was observed (see Table 2).

Table 4 shows the EPR double integrated intensities (DII) of the $V_O^{\cdot}$ signal on sintered and grounded samples. An increase in the paramagnetic oxygen vacancy concentration with Co_3O_4 or ZnO addition was observed. According to the above discussion, cobalt could stabilise as Co^{+2} and zinc as Zn^{+2} producing $V_O^{\cdot\cdot}$ during lattice substitution. After that, $V_O^{\cdot\cdot}$ was transformed to$V_O^{\cdot}$ spending electrons. Then, an increase in the paramagnetic specie ($V_O^{\cdot}$) was observed. On the other hand, a diminution in the paramagnetic oxygen vacancy concentration with manganese addition was produced. According to the above equations, manganese could stabilise as Mn^{+2} and an increase in oxygen vacancies should be observed. It is probable that the single line corresponding to Mn^{+2} masked the $V_O^{\cdot\cdot}$ signal. This fact confirms that Mn^{+2} ions remain at the grain boundaries acting as densifying agent of SnO_2 powders. Also, lines with hyperfine structure due to Mn^{+4} in the bulk were detected. The broad line corresponding to Mn_2O_3[23] was not observed. The notable increasing in the $V_O^{\cdot}$ concentration with antimony or niobium addition was due to the transformation of $V_O^{\cdot\cdot}$ into $V_O^{\cdot}$.This transformation used the electrons generated in the lattice substitution.

Table 4
Relative EPR double integrated intensities (DII) of $V_O^{\cdot}$ ($g = 1.89$) for the sintered and grounded samples

Sample	DII ($V_O^{\cdot}$) / DII ($V_O^{\cdot}$) in sample Sn
Sn	1
SnCo	3.37
SnZn	1.23
SnMn	0.19
SnCoSb	202.6
SnCoNb	328.9

Fig. 1 shows SEM microstructures of the sintered samples and Table 5 lists their mean grain sizes. Different sintered microstructures with the oxide addition were obtained. Tin oxide samples (Sn) showed a porous structure (low density), small grain size (0.5 μm) and agglomerates close to 5 μm, indicating a small sinterisation without dopant addition. In this case, the low sinterability is related to the low self-diffusion coefficient of Sn^{+4} and O^{-2} in SnO_2 and to the vapour pressure of SnO_2 at sintering temperatures favouring non-densifying mechanisms as evaporation–condensation.[20] The addition of several dopants favours the oxygen vacancies formation and allows the grain growth through a solid-state diffusion mechanism.[14] From Fig. 2, a high electrical conduction in sample Sn was observed. The small grain size, registered in this sample, favoured the intergranular barrier overlapping after the slow cooling process from the sintering temperature. These overlapped barriers improved the electrical conduction

Samples with zinc (SnZn) showed densities close to the theoretical density (Table 2) and an homogeneous grain microstructure with a mean grain size of 3 μm. In these samples non secondary phases were observed by SEM. Notable grain growth in these samples was produced by oxygen vacancies formation during the ions substitution (Table 5). From Fig. 2 an important diminution in the sample conductivity with ZnO addition was observed. This diminution was due to the homogeneous microstructure, and to the increase in the effective barrier voltage value due to the dopant substitution (Table 5). These barriers decreased the electrical conduction in the prebreakdown region. These samples also presented the higher breakdown electrical field (Table 5).

Samples with Co_3O_4 produced samples with an intermediate conduction between Sn and SnZn, a breakdown electrical field of about 920 V/cm and a grain size range of 1–20 μm. This wide grain size distribution was caused by a non-homogeneous dopant substitution in the sample. The apparition of big grains produced a reduction in the breakdown electrical field and increased the sample conductivity. Also, a diminution in the V_g respect to sample SnZn was registered. This change could be attributed to a more effective substitution in the sample with ZnO.

Manganese addition produced an important grain growth (mean grain size 8.2 μm with grains as large as 20 μm) indicating that another sintering mechanism appears. Gouvea et al.[24] did not find a liquid formation by TEM. They considered that the low solubility cannot affect significantly the intrinsic disorder of SnO_2 at high temperature. Consequently, they did not consider an improvement of volume diffusion due to Mn dissolution. They determined that the matter transport occurs only at the grain surfaces when the surface manganese

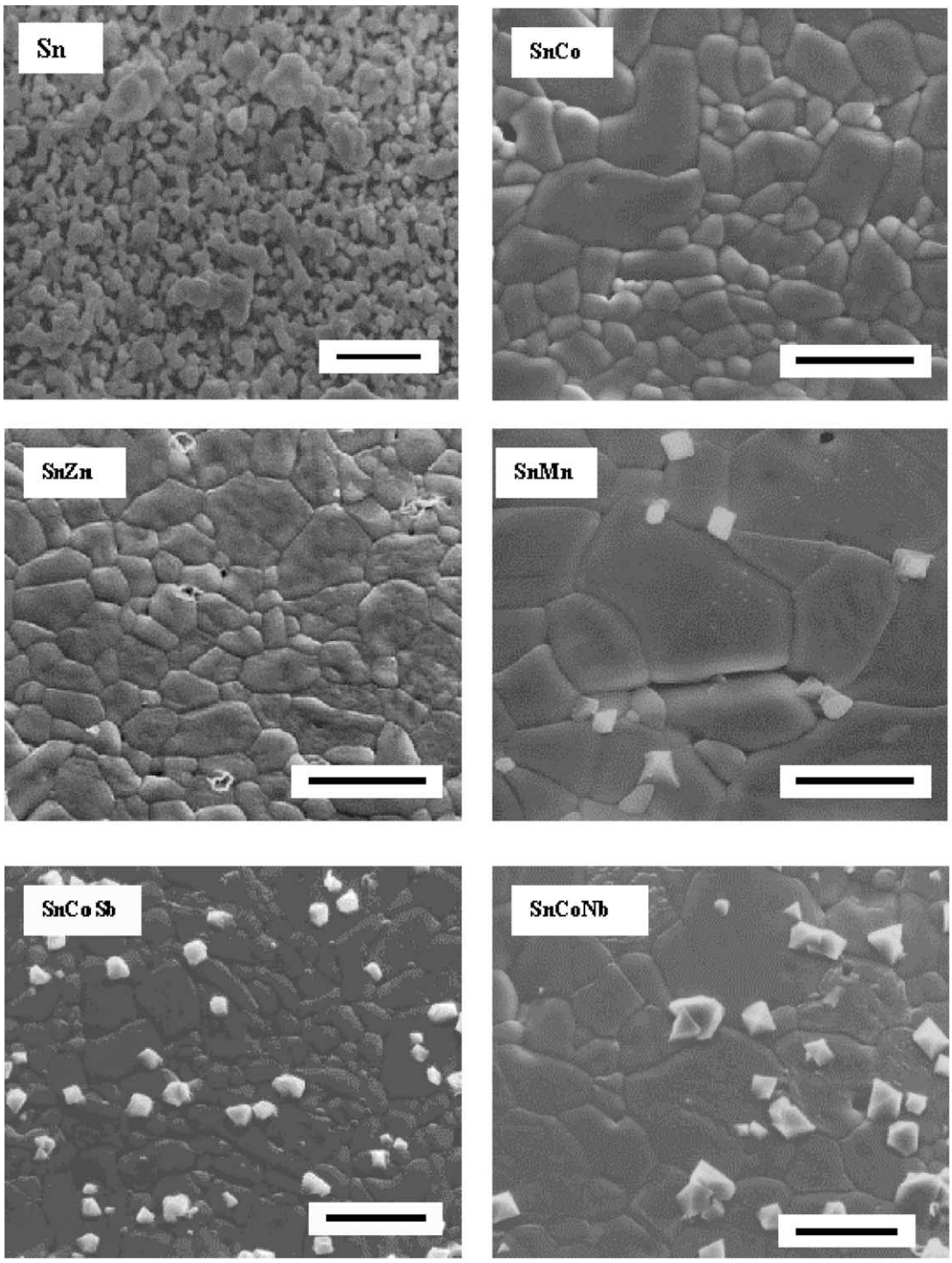

Fig. 1. SEM microstructure of the sintered samples. Bar = 10 μm.

concentration is lower than a critical value estimated as 5×10^{-6} mol m^{-2}. When the Mn surface concentrations is larger than the critical concentration the thickness of the segregation layer would be larger to provoke the diffusion in a volume localised around the grains and not only on the surface. In these samples a secondary phase at the grain boundaries was detected by SEM. Analyses performed by EDS showed that this phase has Sn and Mn in a relation close to 1:11.5. Early papers presented the possible apparition of Mn_2SnO_4 and/or Mn_2O_3 phases in tin oxide varistors[24] but by EPR analysis the presence of Mn_2O_3 particles was not detected in this study. It is probable that the secondary phase composition is close to MnO with a small quantity of Mn_2SnO_4. From Fig. 2 and Table 5 an important diminution in the electrical conductivity, a reduction in the grain voltage (V_g) and

Table 5
Mean grain size, number of barriers, breakdown field, grain voltage and effective voltage value of the samples

Sample	Mean grain size (μm)	Number of barriers	Breakdown field (V/cm)	Grain voltage (V_g)	Effective barrier voltage value (%)
Sn	0.5	3000	1000	0.05	1.4
SnCo	4.8	312	920	0.44	12.6
SnZn	3.0	500	2300	0.69	20.0
SnMn	8.2	183	2000	1.64	47.0
SnCoSb	3.1	483	400	0.124	3.5
SnCoNb	6.5	231	600	0.39	11.4

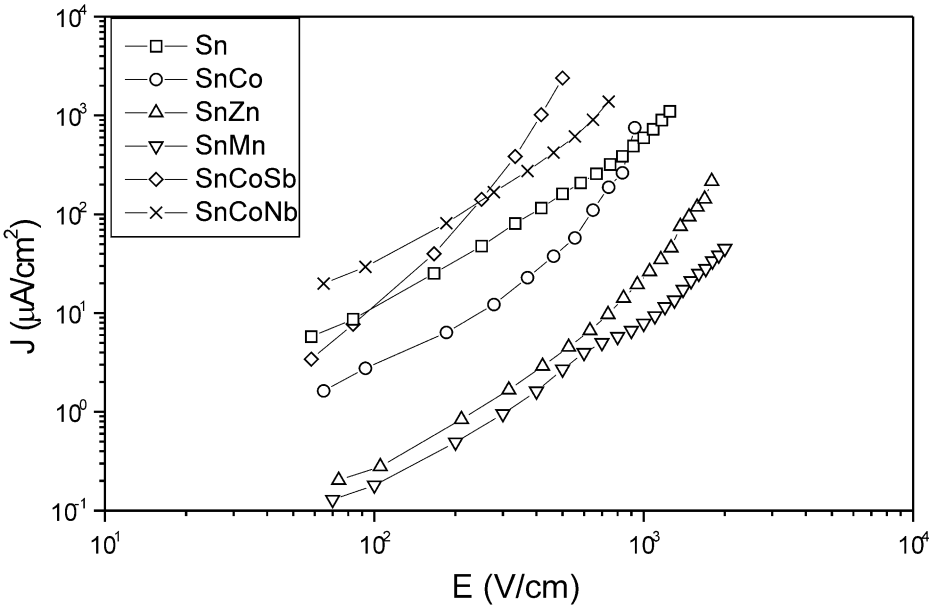

Fig. 2. Density current against applied voltage field curves.

an increasing in the breakdown electrical field were registered. The more effective barrier voltage in this sample was due to a more effective dopant substitution. Also the presence of secondary phases at the grain boundaries could influence the electrical conduction.

In samples with Co_3O_4, ZnO or MnO_2 segregated ions to the grain boundaries contributed to the potential barrier formation at the grain boundaries. These barriers were responsible of the varistor non-ohmic properties. Also, the presence of precipitated secondary phases in sample with manganese could modify the electrical behaviour.

Samples with antimony addition showed small grains (between 0.5 and 5 μm), and precipitated particles of a secondary phase at the grain boundaries. An analysis by EDS of the secondary phase indicated the presence of Co and Sn in a relation 1:1.1, permitting to conclude that the chemical composition of this phase is close to $CoSnO_3$. The notable reduction in the grain size was due to the possible effect of the secondary phase inhibiting the grain growth, and to the reduction in the total oxygen vacancy concentration by the oxygen produced in the antimony substitution [Eq. (23)], and by the cobalt solution in the secondary phase.

Samples with niobium addition showed grain sizes between 3 and 20 μm, and the presence of a secondary phase. Analysis by EDS showed that the secondary phase was composed by Sn and Co in a relation 1:1.4, indicating that the precipitated secondary phase composition was intermediate between $CoSnO_3$ and Co_2SnO_4. In these samples Nb^{+5} substituted Sn^{+4} in the SnO_2 lattice and segregated cobalt at the interface forming secondary phase particles.

On the other hand, Sb_2O_3 or Nb_2O_5 addition produced an increment in the samples conductivity and a diminution in the breakdown electrical field (Table 5), due to electrons produced in the ion substitution [see Eqs. (23) and (26)]. Moreover, samples with Sb_2O_3 presented small grains (between 0.5 and 5 μm) which favoured the intergranular barriers overlapping.

4. Conclusions

The experimental results lead to the following conclusions.

1. From the lattice volume distortion and the substitution equations it is possible to conclude that cobalt, zinc and manganese were stabilised as Co^{+2}, Zn^{+2}, Mn^{+2} in SnO_2 varistors, increasing the oxygen vacancy concentration.
2. The increase in the oxygen vacancy concentration could be responsible for an increasing in the densification and grain growth.
3. Manganese addition provoked an important grain growth and the formation of precipitated particles with a composition close to MnO. Also, manganese was segregated at the grain boundaries and the matter transport concerned the solid/gas interface and the grain boundaries.
4. Niobium or antimony addition to samples with cobalt favoured the formation of particles of a composition close to $CoSnO_3$ with antimony addition or intermediate between $CoSnO_3$ and Co_2SnO_4 with niobium addition. This secondary phase and the annihilation of the oxygen vacancy concentration decreased the grain growth of the samples.
5. Co_3O_4, ZnO, and MnO_2 improved the current density vs. electrical field characteristics due to the increasing in oxygen vacancies concentration and to the substitution of tin ions by added metal (M''_{Sn}, Mn'_{Sn}).

Acknowledgements

The authors acknowledge the National Agency of Scientific and Technological Promotion (ANPCyT) for partial support of this research.

References

1. Levinson, L. M. and Philipp, H. R., Zinc-oxide varistors-a review. *Am. Ceram. Soc. Bull*., 1986, **65**, 639–646.
2. Matsuoka, M., Progress in research and development of zinc oxide varistors. In *Grain Boundary Phenomena in Electronic Ceramics, Advances in Ceramics*, ed. L. M. Levinson. The American Ceramic Society Inc, Ohio, 1981, pp. 290–308.
3. Gupta, T. K., Application of zinc oxide varistors. *J. Am. Ceram. Soc*., 1990, **73**, 1817–1840.
4. Hozer, L., *Semiconductor Ceramics, Grain Boundary Effects*. Ellis Horwood Series in Physics and its Applications, Poland, 1994, pp. 44–108
5. Ichinose, N. and Watanabe, M., VDR effect in Bi diffused $SrTiO_3$ based ceramics. In *Grain Boundaries and Interfacial Phenomena in Electronic Ceramics, Ceramic Transactions*, ed. L. M. Levinson and S. Hirano. The American Ceramic Society Inc, Ohio, 1994, pp. 231–238.
6. Yang, S. L. and Wu, J. M., Effects of Nb_2O_5 in (Ba, Bi, Nb)-added TiO_2 ceramic varistors. *J. Mater. Res*., 1995, **10**, 345–351.
7. Yan, M. F. and Rhodes, W. W., Varistor properties of (Nb,Ba)-doped TiO_2. In *Grain Boundaries in Semiconductor, Materials Research Society Proceeding*, ed. H. J. Leamy, G. E. Pike and C. H. Seager. North Holland, New York, 1982, pp. 357–362.
8. Pianaro, S. A., Bueno, P. R., Longo, E. and Varela, J. A., A new SnO_2-based varistor system. *J. Mat. Sci.Lett*., 1995, **14**, 692–694.
9. Pianaro, S. A., Bueno, P. R., Longo, E. and Varela, J. A., Microstructure and electric properties of a SnO_2 based varistor. *Ceram. Int*, 1999, **25**, 1–6.
10. Castro, M. S. and Aldao, C. M., Characterization of SnO_2 varistors with different additives. *J. Eur. Ceram. Soc*., 1998, **18**, 2233–2239.
11. Pianaro, S. A., Bueno, P. R., Olivi, P., Longo, E. and Varela, J. A., Effect of Bi_2O_3 on the microstructure and electrical properties of the SnO_2–CoO–Nb_2O_5 varistor system. *J. Mat. Sci. Lett*., 1997, **16**, 634–638.
12. Madou, M. J. and Morrison, R., *Chemical Sensing with Solid State Devices*. Academic Press, San Diego, 1989.
13. Moseley, P. T., Solid state gas sensors. *Meas. Sci. Technol*, 1997, **8**, 223–237.
14. Varela, J.A., Perazolli, L.A., Longo, E., Leite, E.R. and Cerri, J.A., Effects of atmosphere and dopants on sintering of SnO_2. In *Radiation Effects and Defects in Solids,* vol. 146, Gordon and Breach Science Publishers, India, 1998, pp. 131–147.
15. Dolet, N., Heintz, J. M., Rabardel, L., Onillon, M. and Bonnet, J. P., Sintering mechanisms of $0.99SnO_2$-0.01CuO mixtures. *J. Mat. Sci*., 1995, **30**, 365–368.
16. Duvigneaud, P.H. and Reinhard, D., Activated sintering of tin oxide. In *Science of Ceramics,* vol. 12, Ceramurgia s.r.l., Faenza, Italy, 1980, pp. 287–292.
17. Pianaro, S. A., Bueno, P. R., Olivi, P., Longo, E. and Varela, J. A., Electrical properties of the SnO_2-based varistors. *J. Mat. Sci.: Mat. Electron*, 1998, **9**, 159–165.
18. Cullity, B. D., *Elements of X-Ray Diffraction*. Addison Wesley, USA, 1978, p. 501.
19. Murugaraj, P., Kutty, T. R. N. and Subba Rao, M., Diffuse phase transformations in neodymium-doped $BaTiO_3$ ceramics. *J. Mat. Sci*., 1986, **21**, 3521–3527.
20. Leite, E. R., Nascimento, A. M., Bueno, P. R., Longo, E. and Varela, J. A., The influence of sintering process and atmosphere on the non-ohmic properties of SnO_2 based varistors. *J. Mat. Sci.: Mat. Electron*, 1999, **10**, 321–327.
21. *Handbook of Chemistry and Physics (56th ed.)*. CRC Press, Ohio, 1974.
22. Ovenston, A., Sprînceanâ, D., Walls, J. R. and Câldâraru, M., Effects of frequency on the electrical characteristics of tin-antimony-oxide mixtures. *J. Mat. Sci*., 1994, **29**, 4946–4952.
23. Las, W. C., Gouvea, D. and Sano, W., EPR of Mn as densifying agent in SnO_2 powders. *Solid State Science*, 1999, **1**, 331–337.
24. Gouvea, D., Smith, A., Bonnet, J. P. and Varela, J. A., Densification and coarsening of SnO_2-based materials containing manganese oxide. *J. Eur. Ceram. Soc*., 1998, **18**, 345–351.